Nonlinear Modeling of the Heat Transfer in Loudspeakers

Wolfgang Klippel

Klippel GmbH
Dresden, 01277, Germany
www.klippel.de

ABSTRACT

Traditional modeling describes the heat flow in loudspeakers by an equivalent circuit using integrators with different time constants. The parameters of the lumped elements are assumed to be independent of the amplitude of the signal. This simple model fails in describing the air convection cooling which becomes an effective cooling mechanism if the velocity of the coil and/or the velocity of the forced air in the gap becomes high. This paper presents a large-signal model considering the nonlinear interactions between the electro-mechanical and thermal mechanisms. The model and parameters are verified by practical measurements on the drivers. The dominant paths for the heat flow are identified and means for increasing the power handling capacity are discussed.

1 Introduction

Transducers have a relatively low efficiency in the conversion of an electric input into mechanical or acoustical output and most of the energy heats up the voice coil. Although some materials can handle high temperatures ($T_v > 250$ K) the heating is probably the most important factor limiting the output. For driver and system designers all means are welcome that keep the coil temperature below the critical value. Increasing the efficiency reduces primary heating. There are ways to bypass some power around the coil or to improve the cooling of the coil at least. Even if we can not improve the long-term power handling we may increase the thermal capacity of the coil to cope with short power peaks.

To do the right things we have to understand the complex mechanisms affecting voice coil temperature. There are not only electrical, mechanical and thermal processes in the driver, but also the influences of the loudspeaker system due to the enclosure and crossover. The properties of the signal also have to be considered. A phyiscal model is required which can be fitted to a particular loudspeaker by measuring a few parameters. Such an identified model is the basis for predicting the mechanical and thermal behavior of the loudspeaker for any audio signal used. Such a physical model is not only useful for the analysis and optimization of the heat transfer but also for designing electronic control circuits giving reliable protection against thermal overload.

This paper follows this target. At the beginning the results of the traditional thermal modeling are summarized and the limits are discussed. Later an extended model is presented and verified by systematic measurements. Finally a simple technique for measuring the parameters of the nonlinear model is suggested and the application is discussed on practical examples.

2 Glossary of Symbols

The following symbols are used within the paper.

State Variables:

i	input current at terminals
u	voltage at terminals
x	voice coil displacement
v	velocity of voice coil
i_2	current in resistance R_2 representing losses due to eddy currents
P_{Re}	power dissipated in R_e
P_{R2}	power dissipated in R_2
P_{coil}	power dissipated in voice coil + former
P_{mag}	power dissipated in magnet due to eddy currents
P_{ev}	power supplied to voice coil due to eddy currents
P_{em}	power supplied to magnet due to eddy currents
P_{con}	power supplied to ambience due to convection cooling
P_t	power transformed into minimum impedance of the warm driver
P_e	rated power transformed into minimum impedance of the cold driver
T_v	temperature of the voice coil
T_m	temperature of the magnet structure
T_{vss}	steady-state temperature of voice coil in thermal equilibrium
T_{mss}	steady-state temperature of magnet in thermal equilibrium
ΔT_v	increase of voice coil temperature $\Delta T_v(t)=T_v(t)-T_a$
ΔT_m	increase of the temperature of magnet structure and frame $\Delta T_m(t) = T_m(t)-T_a$
T_a	temperature of the cold transducer (ambient temperature)

γ factor describing the fraction of input power bypassing the voice coil

Electromechanical Parameters:

$R_e(T_v)$ electrical voice coil resistance at DC depending on voice coil temperature

$R_e(T_a)=R_e$ electrical voice coil resistance at DC of cold coil

L_e voice coil inductance at low frequencies

L_2 para-inductance at high frequencies

R_2 resistance due to eddy currents

M_{ms} mechanical mass of driver diaphragm assembly including air load and voice coil

R_{ms} mechanical resistance of total-driver losses

$K_{ms}(x)$ mechanical stiffness of driver suspension

$C_{ms}(x) = 1 / K_{ms}(x)$ mechanical compliance of driver suspension

$Bl(x)$ force factor (Bl product)

$F_m(x,i)$ reluctance force due to variation of $L_e(x)$

f_s resonance frequency of the mechanical system

Z_{min} minimum impedance

ρ_0 density of air (=1.18 kg /m^3)

c speed of sound in air

Thermal Parameters:

R_t total thermal resistance of path from coil to ambience

R_{tv} thermal resistance of path from coil to magnet structure due to conduction

R_{tm} thermal resistance of magnet structure to ambient air

C_{tv} thermal capacitance of voice coil and nearby surroundings

C_{tm} thermal capacitance of magnet structure

$R_{tc}(v)$ thermal resistance of path from coil to air in the gap due to convection cooling

$R_{ta}(x)$ thermal resistance of path from air in the gap to ambience due to convection cooling

$R_{tt}(v)$ thermal resistance of path from air in the gap to the magnet structure due to convection cooling

C_{ta} thermal capacitance of enclosed air in convection cooling

m_{air} mass of enclosed air involved in convection cooling

α factor describing the distribution of heat caused by eddy currents on voice coil and magnet

r_v convection cooling parameter considering the cone velocity

r_x convection cooling parameter considering the effect of cone displacement

δ thermal conductivity parameter (δ=0.039 for copper)

r_{vo} convection parameter of a driver with open vent

r_{vs} convection parameter of a driver with sealed vent

A_{vo} sectional area of the vent used for ventilation

τ_v time constant of the voice

τ_m time constant of the magnet frame

Variables used in power test:

ΔT_{on} maximal voice coil temperature ΔT_v during the ON-phase of the power test cycle

ΔT_{off} voice coil temperature ΔT_v measured in the OFF-phase of the power test cycle

t_{on} duration of the ON-phase of the power test cycle

t_{off} duration of the OFF-phase of the power test cycle

t_{tau_v} time in the last off-phase when temperature decayed to ΔT_{tau_v}

t_{s_off} time when the last off-phase starts

t_{start} starting time of the measurement

t_{tau_v} time when the temperature is equal to ΔT_{tau_m}

ΔT_{tau_m} threshold temperature used for assessing τ_m

ΔT_{tau_v} threshold temperature used for assessing τ_v

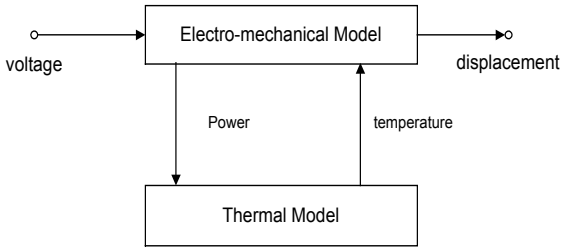

Fig. 1: Interaction between the linear electro-mechanical and thermal model

3 Linear Modeling

The traditional modeling uses an electromechanical and a separated thermal model as shown in Fig. 1. At lower frequencies where the wavelength is large compared with the geometrical dimensions we can use a lumped elements model having only a few number of free parameters. In the traditional approach most of the parameters are assumed as constant but only the voice coil resistance $R_e(T_v)$ depends on the instantaneous voice coil temperature T_v. Fortunately, the variation of the temperature is relatively slow compared with the lowest frequency component used in the loudspeaker. Thus, the electro-mechanical model is considered as a linear but time-variant system which can be investigated by straightforward tools.

The thermal model describes the relationship between power P_t dissipated into heat and voice coil temperature T_v. At very low frequencies close to DC the power P_t would be identical with the power

$$P_{\mathrm{Re}} = \frac{u^2}{R_e(T_v)} \tag{1}$$

dissipated in the DC voice coil resistance $R_e(T_v)$ depending on the voice coil temperature T_v the voltage u at the terminals. Button [4] suggested to use instead of R_e the minimal impedance $Z_{min}(T_v)$ in

$$P_t = \frac{u^2}{Z_{\min}(T_v)} \tag{2}$$

to consider some effects of the losses due to eddy currents and magnetization in the pole plate and magnet. Clearly this rating is only precise at one frequency point above the resonance frequency.

The relationship between voice coil temperature T_v and input power P_t can be modeled by a second-order integrator as shown in Fig. 2. The first integrator represents the heating of the coil by using the thermal resistance R_{tv} and the thermal capacity C_{tv}. The heat transfer from the magnet to the ambience is modeled by a second integrator formed by the resistor R_{tm} and capacity C_{tm}. Two integrators are sufficient for transducers in free air or mounted in a vented enclosure. For a small sealed enclosure Behler [1] suggested a third integrator switched in series to the other ones.

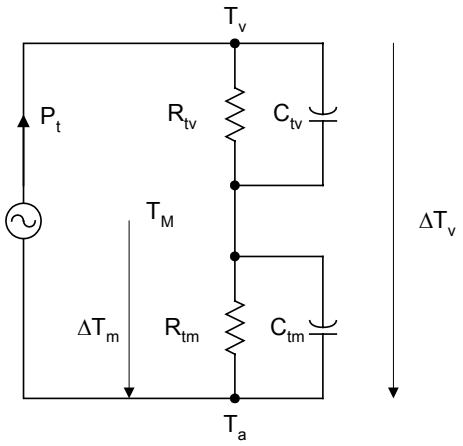

Fig. 2: Traditional Thermal Model

In the following modeling we also need the increase of the voice coil temperature $\Delta T_v(t)=T_v(t)-T_a$ and magnet temperature $\Delta T_m(t)=T_m(t)-T_a$, which is the difference between the absolute temperatures T_v and T_m, respectively, and the ambient temperature T_a.

3.1 Steady-State Behavior

Applying a stimulus with constant power P_t to the driver the thermal system will go into a thermal equilibrium. Since no heat flows in or out of capacitors C_{tv} and C_{tm} the thermal resistances R_{tv} and R_{tm} determine the steady-state voice coil temperature

$$\Delta T_{vss} = (R_{tv} + R_{tm})P_t = R_t P_t \tag{3}$$

and the steady-state magnet temperature

$$\Delta T_{mss} = R_{tm} P_t . \tag{4}$$

3.2 Linear Dynamics

If we vary the input power P_t and observe the variation of the temperature $\Delta T_m(t)$ and $\Delta T_v(t)$ versus measurement time t we see the effect of the thermal capacities C_{TV} and C_{TM}.

After switching on the input power $P_t=P_{on}$ at the time $t=t_{s\_on}$ the temperature ΔT_m of the magnet increases by an exponential function

$$\Delta T_m(t) = \Delta T_{mss}\,(1 - e^{-(t-t_{S\_on})/\tau_m}) \tag{5}$$

to the steady-state temperature ΔT_{mss}. The time constant of the magnet structure is

$$\tau_m = R_{tm} C_{tm} . \tag{6}$$

After switching off the input power at the time $t=t_{s\_off}$ the temperature difference between voice coil and frame/magnet

$$\Delta T_v(t) - \Delta T_m(t) = (\Delta T_{vss} - \Delta T_{mss})\; e^{-(t-t_{S\_off})/\tau_v} \tag{7}$$

decreases by an exponential function with the time constant

$$\tau_v = R_{tv} C_{tv} . \tag{8}$$

3.3 Thermal Power Compression

The increase of the voice coil temperature ΔT_v has an influence on both the electro-mechanical and the thermal model. Since the temperature T_v reduces the half-space efficiency of the driver defined by

$$\eta_0(T_v) = \frac{\rho_0}{2\pi c}\frac{(Bl)^2}{R_e(T_v)}\frac{S_D^2}{M_{ms}^2} . \tag{9}$$

and the input power P_t defined by Eq. (2), we get a natural compression effect in the sound pressure output and in the state variables displacement, velocity and voice coil temperature.

Following the approach proposed by Button [4] we summarize here the most important results:

First we use the thermal coefficient of conductivity δ to describe the relationship between voice coil resistance R_e and voice coil temperature

$$R_e(T_A + \Delta T_v) = R_e(T_A)(1 + \delta \Delta T_v) . \tag{10}$$

We find δ=0.0393 K^{-1} for copper and δ=0.0377 K^{-1} for aluminum. Behler [1] also suggested an additional quadratic term to describe the relationship more precisely. However, impurities in material

and processing of the metal (warm or cold rolling of the copper wire) may cause significant variations. In consideration of those uncertainties any higher-order approximations seems questionable.

Combining Eqs. (2), (3) and (10) we get the implicit relationship

$$\Delta T_v = \frac{U^2 R_t}{Z_{\min}(T_a) + R_e(T_a)\delta\Delta T_v} \tag{11}$$

corresponding with the feedback loop as shown in Fig. 1. Solving this equation we get a nonlinear relationship

$$\Delta T_v \approx \frac{Z_{\min}(T_a)}{2\delta R_e(T_a)}\left(\sqrt{1+\frac{4U^2 R_t \delta R_e(T_a)}{Z_{\min}(T_a)}}-1\right). \tag{12}$$

to the voltage U. Whereas the temperature rises with the squared voltage U^2, at lower values we find a linear relationship $\Delta T_v \sim U$ for $\Delta T_v > 250$ K. This effect gives some relief in the heating of the coil supposed the driver can handle such high temperatures.

Button [4] also predicted the sound pressure level

$$SPL = 112 + 10\log(\eta_0(T_a)) - 10\log\left(\frac{R_t(1+\delta\Delta T_v)}{\Delta T_v}\right) \tag{13}$$

as a function of the voice coil temperature ΔT_v using the efficiency of the cold coil and constant parameters R_t and λ. Taking ΔT_v to infinity we get a maximal SPL output

$$SPL_{\max} = 112 + 10\log(\eta_0(T_a)) - 10\log(R_t\delta) \tag{14}$$

depending only on efficiency of the cold driver, the thermal resistance R_t and the thermal coefficient of conductivity δ. Thus even a stimulus at extremely high voltage will only give a limited output under steady-state condition due to the compression of both input power and efficiency.

The last term in Eq. (13) is the power compression factor

$$PC = 10\log\left(\frac{R_t(1+\delta\Delta T_v)}{\Delta T_v}\right) \tag{15}$$

which describes the loss of output power of the hot driver compared with the output power of the cold driver.

3.4 Limits of the Linear Modelling

Although the traditional modeling gives a lot of enlightening results the thermal behavior of the real driver is much more complex:

This effect is illustrated in the first experiment performed on example driver A. Three kinds of music interrupted by a short break are used as stimulus in a power test. The increase of the voice coil temperature ΔT_v and the power P_{Re} dissipated on resistance R_e is recorded in Fig. 3.

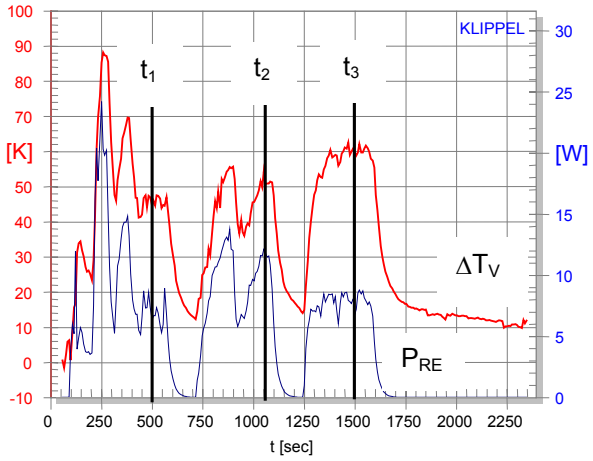

Fig. 3: Voice coil temperature ΔT_v and power P_{Re} versus time while reproducing different music material

Clearly the voice coil temperature follows the power P_{Re} approximately. In the breaks when no power is supplied to the coil, the temperature decays slowly to the ambient temperature. A high time constant is used for the integration of the power to compare the "mean" input power with the steady state temperature at three samples t_1, t_2 and t_3. Here the total thermal resistance is approximated by the ratio $\Delta T_v/P_{Re}$ and listed in Table 1.

Sample	Music	Start [s]	ΔT_v [K]	P_{Re} [W]	$\Delta T_v/P_{Re}$ [K/W]
t_1	Violin concert	0	48	7	6,8
	Break	600			
t_2	Popmusic	700	52	11,5	4,6
	Break	1100			
t_3	Vocal Singer	1250	60	8	7,5
	Break	1550			

Table 1: Total thermal resistance at three different music materials.

Obviously there are significant differences (60 %) in the heat transfer depending on the properties of the signal. Apparently, the high bass content of the popular music compared with the a cappella singer program gives a much better cooling of the coil. This effect is very important but not considered in the traditional modeling. Thus the parameters of the linear model have to be handled as effective parameters and are only valid for a particular stimulus. Thus special kinds of test noise has been defined by national and international committees (IEC 60268, EIA 426) to get some comparability between final products. However, it is questionable how these test signals represent contemporary popular music which almost always evolves more bass. As a second point, the thermal parameters measured of a driver may not

applied to the same driver when mounted in a vented enclosure and operated via a crossover network.

For the evaluation of drivers and for the design of passive and active loudspeaker systems we need driver parameters which are independent on the spectral properties and amplitude of the stimulus. Thus we need more work in the driver modeling to consider the following mechanisms

- dependence of input power on impedance response
- variation input impedance due to driver nonlinearities
- heating process due to eddy currents and magnetization
- cooling process due to air convection
- stalled convection cooling due to amplitude compression of displacement and velocity.

4 Nonlinear Modeling

Nonlinear modeling is a natural extension of the traditional modeling. We still have an electro-mechanical system and a thermal system but both systems are interlaced by multiple state variables as shown in Fig. 4.

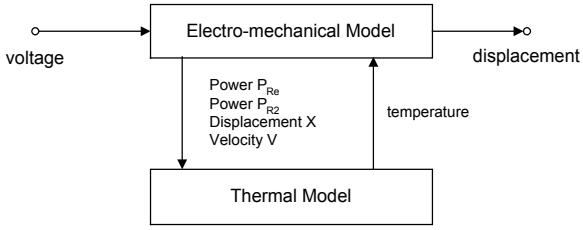

Fig. 4: Interactions between the nonlinear models

In addition to the power P_{Re} and the voice coil temperature ΔT_v in the traditional model in Fig. 1 we find the power P_{R2} dissipated in resistance R_2, displacement x and velocity v of the voice coil. In the following we discuss the process in the two systems separately.

4.1 Electro-mechanical System

We start with the electro-mechanical system because the electrical and mechanical state variables determine how much energy is converted to heat. The equivalent circuit depicted in Fig. 5 describes the large signal behaviour of most transducers over a wide frequency range.

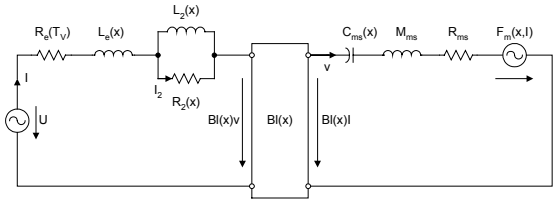

Fig. 5: Lumped-Parameter Model for the electro-mechanical system

In contrast to the linear modeling, the variation of the force factor $Bl(x)$, stiffness $K_{ms}(x)$ and inductance $L_e(x)$ versus displacement x are taken into account. Fig. 6 shows the $Bl(x)$-characteristic for speaker A. The curve is almost symmetrical revealing that the coil has the optimal rest position. Due to the limited height of the coil the force factor decays in a natural way for any positive or negative displacement. The stiffness as shown Fig. 8 increases for any displacement. The minor asymmetry may be caused by the geometry of the pot spider. The inductance has a distinct maximum at negative displacement which is typical for any driver without a shorting ring or copper cap on the pole piece. We assume that the other nonlinear elements $R_2(x)$, $L_2(x)$ representing the para-inductance at higher frequencies have the same shape as curve $L_e(x)$. The nonlinear inductance also produces a reluctance force on the mechanical side which can be interpreted as a electro-magnetic motor force.

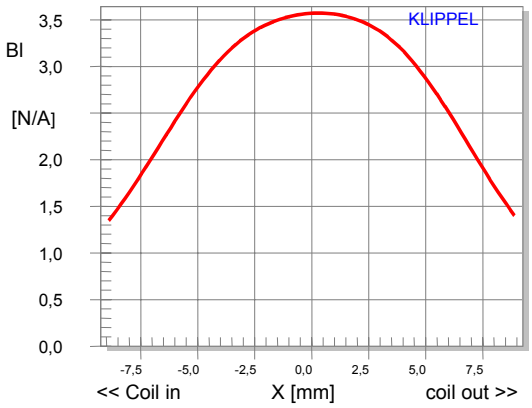

Fig. 6: Force factor $Bl(x)$ versus voice coil displacement x

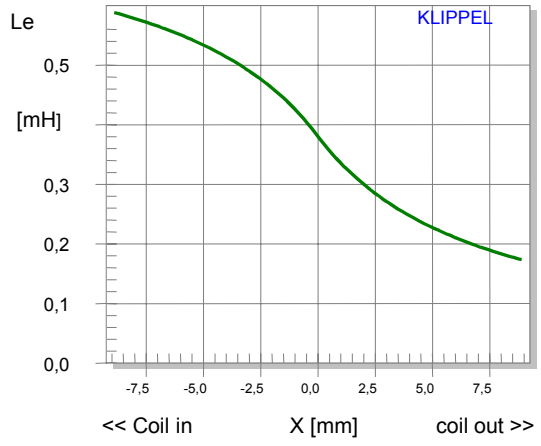

Fig. 7: Voice coil inductance $L_e(x)$ versus displacement x

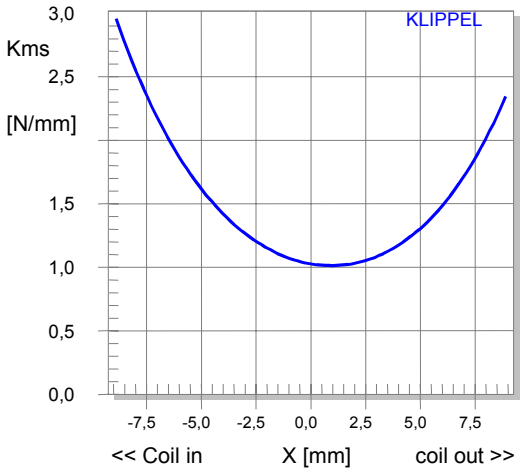

Fig. 8: Stiffness $K_{ms}(x)$ of suspension versus dispacement x

4.1.1 Dynamics of the Mechanical System

In the next step we investigate the behavior of the nonlinear system by exciting with a sinusoidal stimulus. Both the frequency and the amplitude are varied from 5 Hz to 1 kHz. The amplitude of the tone is also varied in 4 steps spaced linearly. Fig. 9 shows the resulting amplitude of the fundamental component of the voice coil displacement. Although the voltage is increased by equal steps the resulting displacement rises at high amplitudes less than at smaller amplitudes. This kind of amplitude compression is not a thermal effect but is caused by the driver nonlinearities.

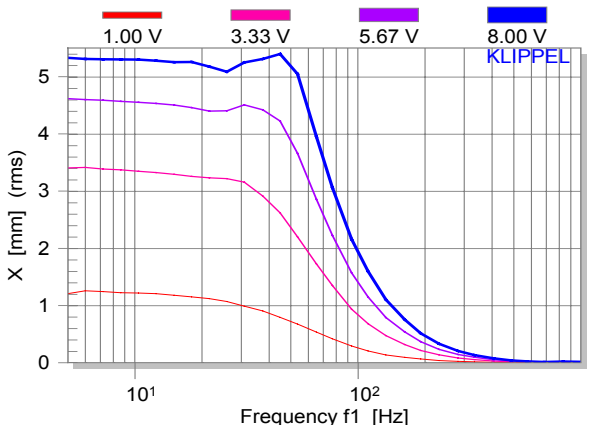

Fig. 9: Voice coil displacement of driver A at ambience temperature for a sinusoidal excitation tone versus frequency f_1 and voltage U_1

Fig. 10 shows the displacement response versus frequency for a constant excitation voltage. A laser triangulation sensor is used to measure the displacement of diaphragm. The measured curve agrees very well with predicted curve using the large signal model as shown in Fig. 5. The third curve represents the results of a linear model using the traditional small signal parameters. Clearly the linear model fails and predicts twice the output of the real speaker at low frequencies. Fig. 11 also reveals a significant loss of velocity due to amplitude compression. This has two effects increasing the final voice temperature:

First, the reduced back EMF will vary the electrical input impedance about the resonance frequency dramatically and will increase the electrical current and the input power P_{Re} as shown in Fig. 12 and Fig. 13, respectively.

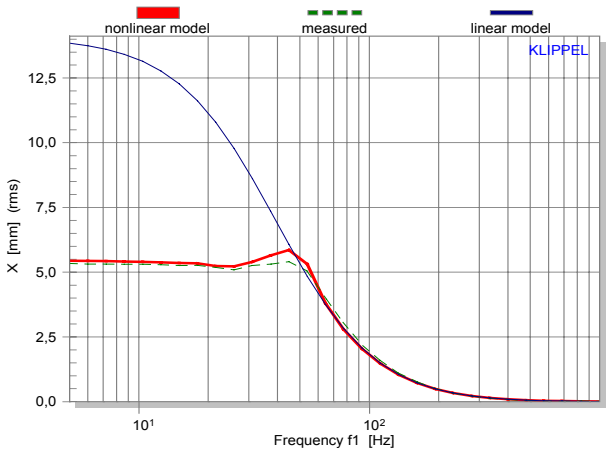

Fig. 10: Voice coil displacement x versus frequency f_1 of driver A at ambient temperature measured (dashed line) and calculated by using a linear model (thin line) and a nonlinear model (thick line).

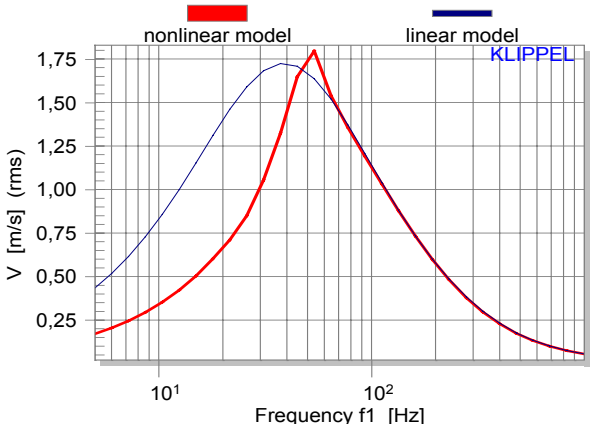

Fig. 11: Voice coil velocity v of driver A at ambient temperature calculated by a linear (thin line) and nonlinear (thick line) model versus frequency f_1

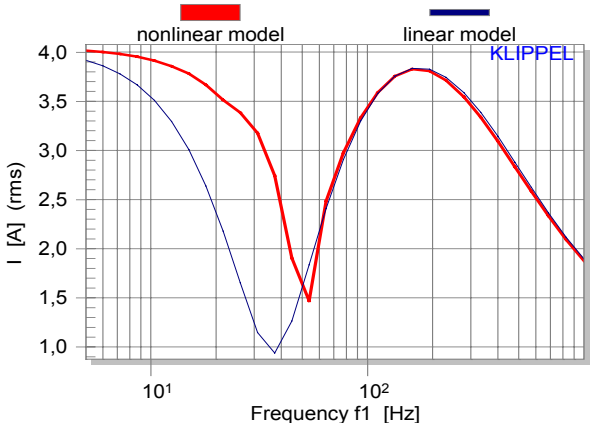

Fig. 12: RMS value of the input current i of driver A at ambient temperature calculated by a linear model (thin line) and a nonlinear model (thick line)

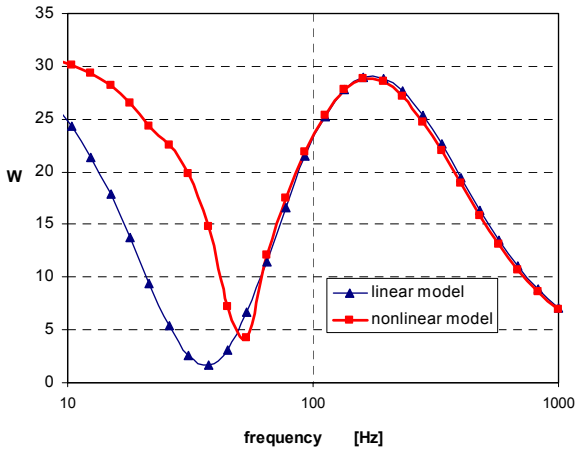

Fig. 13: Input power P_{Re} of driver A at ambient temperature calculated by a linear and nonlinear model

At a frequency of 40 Hz the cold voice coil absorbs 10 times more power as predicted by the linear model.

As a second effect, the amplitude compression will stall the convection cooling. Both effects may cause a significant increase in the voice coil temperature when increasing the signal amplitude. This is important for drivers operated close to the resonance frequency, as in subwoofer systems. Contrary to broad-band systems, where most of the energy is transferred above the resonance, subwoofer drivers can run normally into thermal power compression.

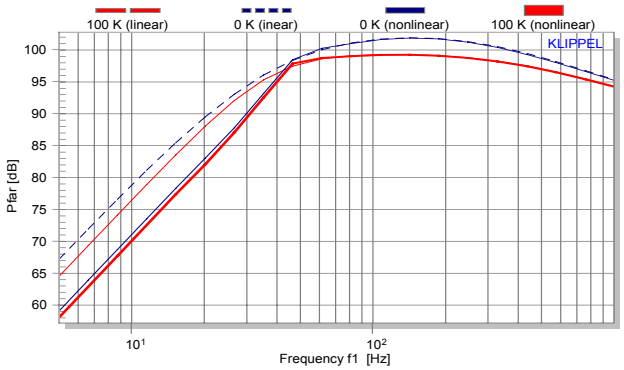

Fig. 14: Sound pressure frequency response of the cold and warm coil predicted by linear and nonlinear model.

Fig. 14 shows the effect of the variation of the voice coil resistance (ΔT_v=0 K and ΔT_v= 100 K) on the sound pressure response by using a linear and a more precise nonlinear model. If the sinusoidal tone f_1 is above the resonance frequency f_s the linear and nonlinear models coincide, giving a power compression PC= 2.9 dB. The power compression decreases at higher frequencies where the inductance contributes significantly to the electrical impedance. Below the resonance frequency the nonlinear model reveals 8 dB less output due to the effect of the driver nonlinearities. However, voice coil heating causes here only half the thermal power compression predicted by a linear model.

If we apply a two-tone signal or any other complex stimulus to the driver we also find nonlinear amplitude compression at higher frequencies. Fig. 15 shows the amplitude response of the first tone (voice tone) with variable frequency f_1 while a second tone (bass tone) at fixed frequency f_2=20 Hz with the same amplitude (U_{rms}= 8V) produces significant displacement.

Clearly the linear model can not show any interactions between the two tones. The frequency responses for the cold and warm coil are represented by dotted and dashed lines in Fig. 15, are identical with the responses in Fig. 14 measured with one tone only. The nonlinear speaker reproduces the voice tone at low and high frequencies significantly lower than the linear speaker. Only above the resonance the nonlinear compliance causes an increase of 2 dB output of the fundamental component of the voice tone. The thermal power compression is almost negligible for frequencies below resonance. Only for frequencies above the resonance, the thermal power compression PC is distinguishable from the linear speaker.

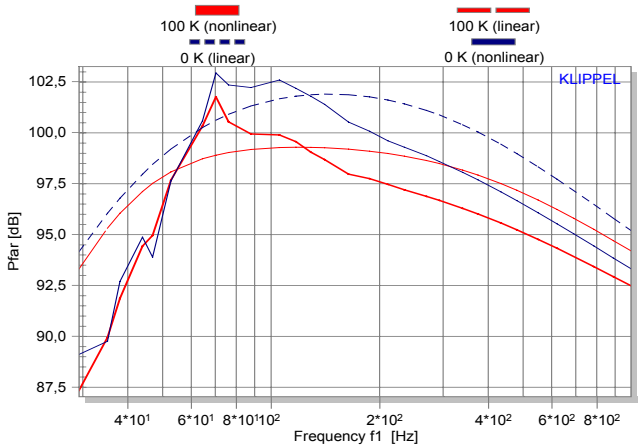

Fig. 15: Amplitude of fundamental sound pressure component versus frequency f_1 of a warm and cold driver excited by a two-tone stimulus (f_1 variable, f_2= 20 Hz, U_1=U_2= 8 V_{rms}) predicted by a linear and nonlinear model.

The effects generated by a two-tone stimulus illustrate the variety of symptoms generated by speaker nonlinearities producing not only harmonic and intermodulation distortion but having also an significant impact on the fundamental output. In contrast to the simplified linear model we can not predict the output by a simple high-pass characteristic but we have to solve the nonlinear parameters with particular driver parameters directly. Numerical tools implemented in a PC make this practicable.

4.2 Nonlinear Thermal Model

After discussing the basic modeling of the electro-mechanical circuit we introduce an extended thermal model as shown in Fig. 16. Comparing it with

Fig. 2 we find the two basic integrators for the voice coil and magnet, represented by R_{tv}, C_{tv} and R_{tm}, C_{tm}, respectively. However, there is an additional branch connected in parallel to both integrators to model the forced convection cooling. This branch comprises thermal resistances $R_{tc}(v)$, $R_{ta}(x)$ and $R_{tt}(v)$ depending on the velocity v and displacement x of the coil. These elements make the thermal model nonlinear. The resistance $R_{tc}(v)$ describes the heat transfer from the coil to the surrounding air within the gap or in vicinity of the pole plate. Some of the heat will be transferred to the pole tips and to the magnet via the resistance $R_{tt}(v)$ but most heat will be transferred via resistor $R_{ta}(x)$ to the ambience. $R_{ta}(x)$ describes the air exchange and depends like a pumping effect on the displacement x and geometry of the vents. In most drivers where the air chamber is not sealed the pumping effect is dominant and the path via resistor R_{tt} can be neglected. The capacity C_{ta} of the air involved in convection cooling is also very small and can be approximated by

$$C_{ta} \approx m_{air} \tag{16}$$

where the equivalent air mass m_{air} is in gram and C_{Ta} is in Ws/Kelvin. This element will be not considered in the further modeling.

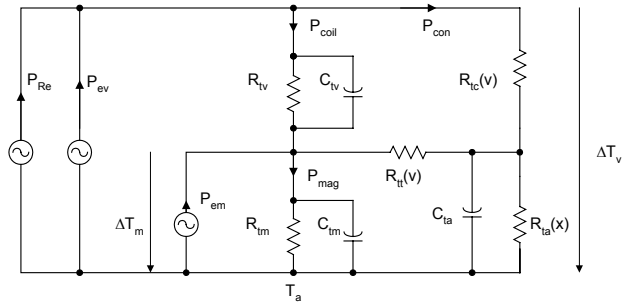

Fig. 16: Nonlinear thermal model

In contrast to the linear model the extended model uses multiple power sources providing heat to different points in the thermal circuit.

The first source

$$P_{\mathrm{Re}} = R_e(T_v)i^2 \tag{17}$$

is the heat dissipated in resistance $R_e(T_v)$ using the input current i. The second power source represents the eddy currents transferred to the voice coil former

$$P_{ev} = \alpha\ P_{R2} \tag{18}$$

with the total power dissipated in the resistor R_2.

$$P_{R2} = R_2 i_2^{\ 2} \tag{19}$$

using the rms-value of the current in R_2

$$i_2 = \frac{i}{\sqrt{1+\left(\frac{R_2}{L_2 2\pi f}\right)^2}} \tag{20}$$

The other part of the power P_{R2} is supplied via the source

$$P_{em} = (1-\alpha)P_{R2} \tag{21}$$

to the pole tips, pole plate and the magnet.

The factor α describes the splitting of power P_{R2}. Clearly we are interested in keeping this value small to transfer as much heat as possible to the magnet and bypass the voice coil.

The bypass power factor

$$\gamma = 1 - \frac{P_{coil}}{P_{\mathrm{Re}} + P_{R2}} \tag{22}$$

describes the ratio of power which is directly transferred to the magnet and the ambience but does not contribute to the heating of the coil.

4.3 Dependency on state variables

Both resistances $R_{tc}(v)$ and $R_{ta}(x)$ depend on the air flow caused by coil movement. $R_{tc}(v)$ describes the first step of the transfer which is directly related to the velocity of the air particles close to the surface of the coil. Since this variable is hard to measure we correlate it to the velocity of the coil and assume a linear relationship between both variables. We also introduce a simple model describing an inverse relationship between resistor

$$R_{tc}(v) = \frac{1}{v_{rms} r_v} \tag{23}$$

and the rms value of the velocity v_{rms} and the convection parameter r_v.

$R_{ta}(x)$ describes the air exchange with the ambience. Clearly not the velocity but more the displacement is important for the pumping effect. We also assume a simple inverse relationship

$$R_{ta}(x) = \frac{1}{x_{rms} r_x} \tag{24}$$

and introduce the convection parameter r_x.

5 Convection Cooling

To verify the assumptions in the modeling, series of special measurements have been performed on a variety of drivers, and the model has then been applied to check for agreement between measured and predicted behavior.

5.1 Measurement Setup

The driver under test is excited by a two-tone stimulus as shown in Fig. 17. A first tone at fixed frequency f_2= 2 kHz is generated to heat the voice coil significantly. Since the resonance frequency of driver A is below 40 Hz the movement caused by this tone is negligible. The frequency f_1 of the second tone is varied during the test in 10 steps spaced logarithmically between 5 and 200 Hz. This signal has been supplied as an external stimulus to the power test module (PWT) of the Distortion Analyzer. The stimulus is switched with a cycle schema having a ON and OFF phase of 2 minutes each. A small pilot tone at 1 Hz frequency is added to the cycled stimulus to measure the voice coil resistance R_e at very low frequencies close to DC. Such AC pilot tone is more convenient than using an additional DC-component because this signal can be supplied via a normal AC-coupled power amplifier to the speaker. This technique also avoids any DC offset of the coil. During the test, current $i(t)$ and voltage $u(t)$ is monitored by special current and voltage sensors and stored in a buffer after 8 seconds. The displacement $x(t)$ is also measured by using the triangulation laser head.

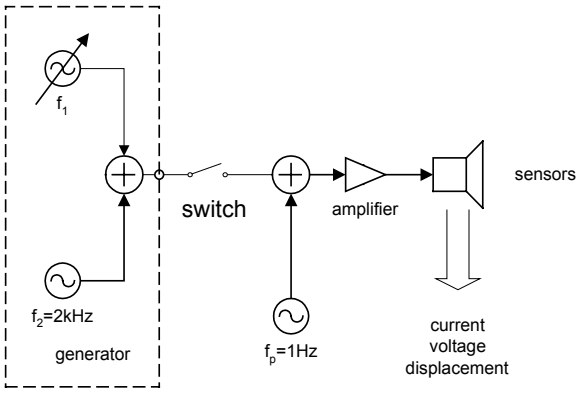

Fig. 17: Measurement setup to measure convection cooling

5.2 Results

Fig. 18 shows the monitored rms-values of voltage and current at the speakers terminals versus measurement time t. Starting at 5 Hz the frequency f_1 is increased after completing an On/Off cycle. Whereas voltage is held constant at 17 V_{rms} during the On-phase the current varies according to the resistance R_e.

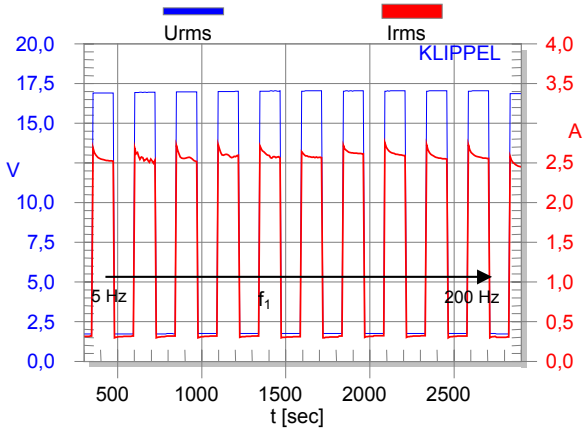

Fig. 18: Voltage U_{rms} (thin line) and current I_{rms} (thick line) of the cycled two-tone signal (f_2=const., f_1= varied from 5 to 200 Hz) versus measurement time.

Using the 1 Hz pilot tone the resistance R_e is calculated during the power test and shown versus time t in Fig. 19.

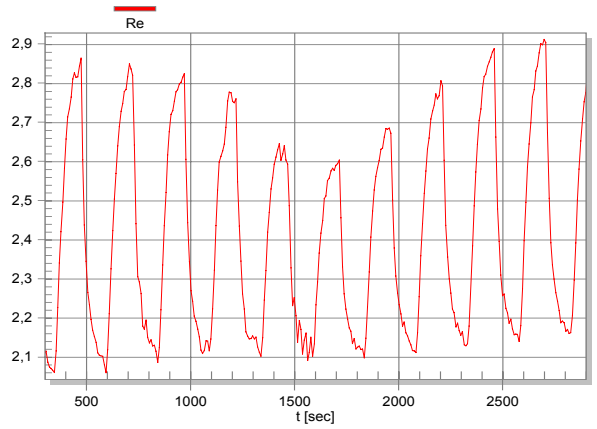

Fig. 19: DC voice coil resistance R_e versus measurement time

The increase of voice coil temperature

$$\Delta T_v = \frac{1}{\delta}\left(\frac{R_e(T_v)}{R_e(T_A)} - 1\right) \tag{25}$$

is calculated from $R_e(T_v)$ by using δ=0.0393 K^{-1} for the known copper coil and the initial resistance $R_e(T_a)$ at ambient temperature.

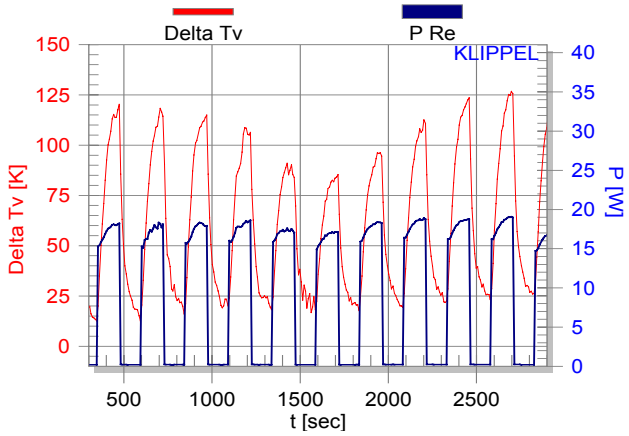

Fig. 20: Voice coil temperature ΔT_v (thin line) and power P_{Re} dissipated in resistance R_e (thick line) versus measurement (varied frequency f_1)

Fig. 20 shows the variation of voice coil temperature and the power P_{Re} versus measurement time. In each OFF-phase when the power P_{Re} is zero the voice coil temperature ΔT_v decreases rapidly to a value T_{min} close to the magnet temperature ΔT_{mss} in steady state. In each ON-phase the voice coil temperature ΔT_v approaches the maximal value T_{max} close to the value ΔT_{vss} of the coil in steady-state condition. During the whole test the magnet gradually increases by about 10 K. To reduce the influence of the thermal dynamics caused by the capacities C_{tv} and C_{tm} we read the maximal variation of the voice coil temperature T_{step}= T_{max}-T_{min} and the power P_{re} at the switching instances of the cycling.

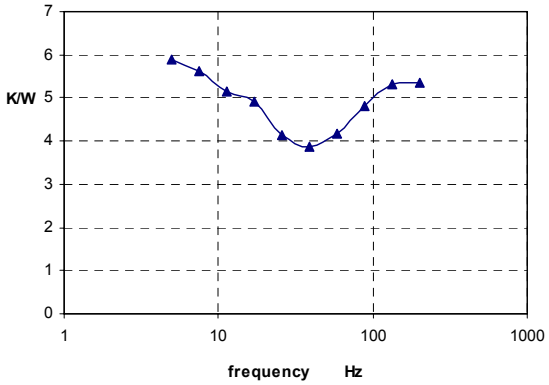

Fig. 21: Increase of the voice coil temperature T_{step} by providing an input power P_{Re} during cycling

The ratio T_{step}/P_{Re} as shown in Fig. 21 describes the parallel connection of R_{tc} and the convection resistance R_{tc} + R_{ta} versus frequency f_1. The thermal resistance reduces by about 30 % at f_1 = 40 Hz compared with very low or high frequencies.

The sum of both convection resistances can be separated from R_{tc} by

$$\left(R_{tc} + R_{ta}\right) = \frac{1}{\frac{P_{\mathrm{Re}}(f_1)}{T_{step}(f_1)} - \frac{1}{R_{tv}}} \tag{26}$$

where resistance R_{tv} = $T_{step}(f_2)/P_{Re}(f_2)$ = *6.2 K/W* of the voice coil is measured by using the high-frequency tone f_2= *2kHz* only.

Fig. 22 shows the measured frequency response of R_{tc} + R_{ta} versus frequency f_1. Clearly this resistance decreases when the amplitudes of velocity and displacement in Fig. 23 rise.

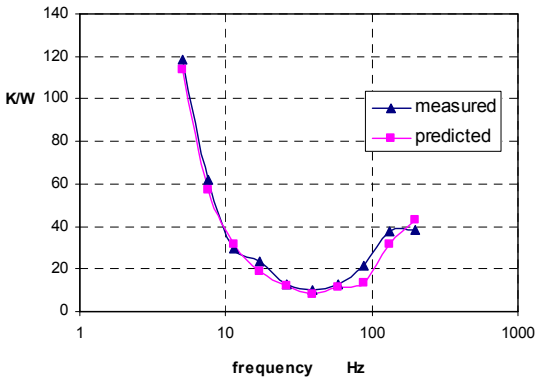

Fig. 22: Measured and predicted total resistance R_{tv}+R_{ta} representing total convection cooling versus excitation frequency f_1

Finally we use the displacement and velocity in Fig. 23 and determine the convection parameters r_v= 0.30 and r_x = 300 in Eqs. (23) and (24) by fitting the predicted to the measured curve in Fig. 22. The agreement is quite reasonable. Fig. 24 shows the resistances R_{tc} and R_{ta} separately. Over the measured frequency range R_{tc} is greater than R_{ta} indicating that the velocity mainly determines the forced convection cooling. R_{ta} rises only at high frequencies because the small displacement can not give sufficient air exchange. In any case, the R_{ta} alone can not model the convection cooling because at low frequencies the air velocity close to the coil is important, not the pumping effect due to high displacement. If the nonlinear model has to be simplified for practical reasons, it seems possible to neglect R_{ta} and to use the velocity dependent resistance R_{tv} only.

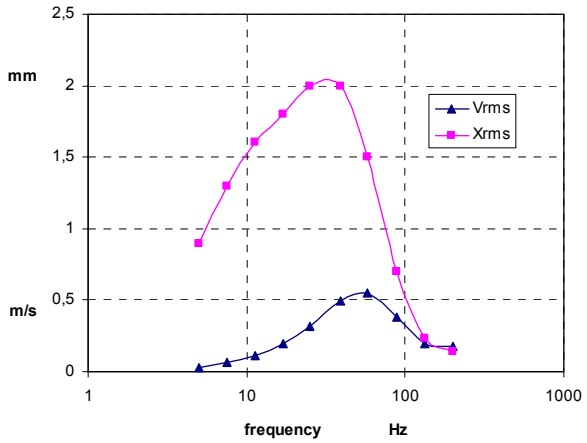

Fig. 23: Voice coil displacement X_{rms} and velocity V_{rms} versus frequency f_1

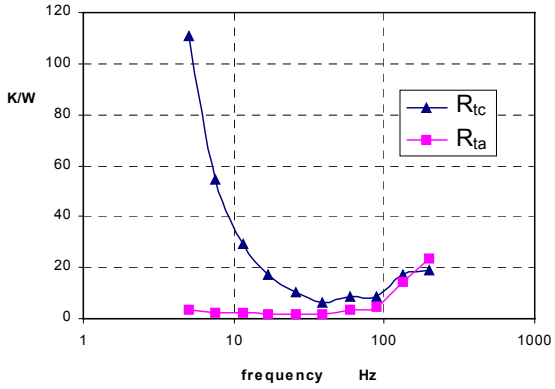

Fig. 24: Thermal resistance $R_{tc}(v)$ and $R_{ta}(x)$ versus frequency f_1 of the excitation signal

6 Measurement of Thermal Parameters

The technique using the two-tone signal has been proven useful for the verification of the model. Beyond loudspeaker research, for loudspeaker development we need a simpler technique that requires less equipment and can be executed in shorter time. We use here a simplified model as shown in Fig. 25.

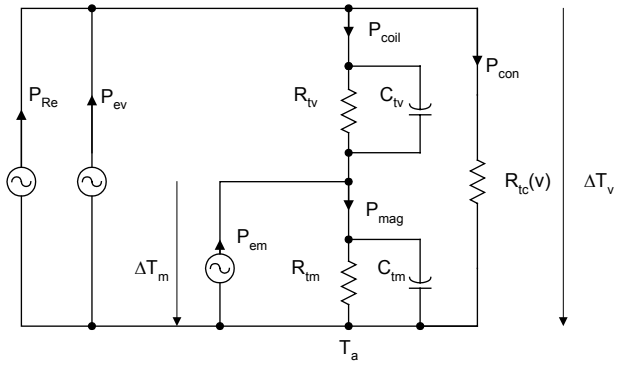

Fig. 25: Simplified thermal model

In contrast to the traditional model in

Fig. 2 we use the velocity dependent resistance $R_{tc}(v)$ for modeling convection cooling. The other parameters R_{ta}, R_{tt}, and C_{ta} are also neglected because in common drivers we have sufficient leakage in the air chamber and $R_{ta} < R_{tv}$ and $R_{tt} >> R_{tv}$.

6.1 Performing the Measurements

Here an alternative technique is suggested performing four measurements. In the first measurement the linear parameters $R_e(T_a)$, L_2 and R_2 are determined from the electrical impedance of the cold driver.

Then three long term power tests are performed using a single tone as stimulus, which is adjusted to the following frequencies:

- $f_1 \approx 10\, f_s$ to measure voice coil and magnet parameters
- $f_2 >> f_1$ to measure direct heat transfer
- $f_3 \approx 1.5\, f_s$ to measure convection parameters

The single tone f_1 in the first power test is set in the middle of the frequency band where the air convection cooling is negligible. The tone f_2 in the second test is set as high as possible to measure the largest effect of the direct heat transfer due to eddy currents. The tone f_3 in the last test is set close but not directly at the resonance frequency f_s to supply sufficient power to the driver.

The stimulus is switched by a cycle scheme (t_{on}=25 min, t_{off}= 5 min). The amplitude of the stimulus is adjusted to the particular driver to get sufficient heating while avoiding thermal or mechanical damage. The duration of the power test should be sufficiently long ($> 4\,\tau_m$) to have the magnet and frame in thermal equilibrium.

During the test the rms-value of the input current $i_{rms}(t)$ and voice coil resistance $R_e(t)$ is monitored and recorded with sufficient temporal resolution. For the third stimulus $f=f_3$ the rms-value $x_{rms}(f_3)$ of the voice coil displacement is also measured.

6.2 Reading Temperature Variations

After performing all three power tests the instantaneous voice coil temperature $\Delta T_v(t)$ is calculated by using Eq. (25) and the conductivity δ appropriate for the coil material. Fig. 26 shows the temperature $\Delta T_v(t)$ and power P_{Re} during the first power test performed on example driver A.

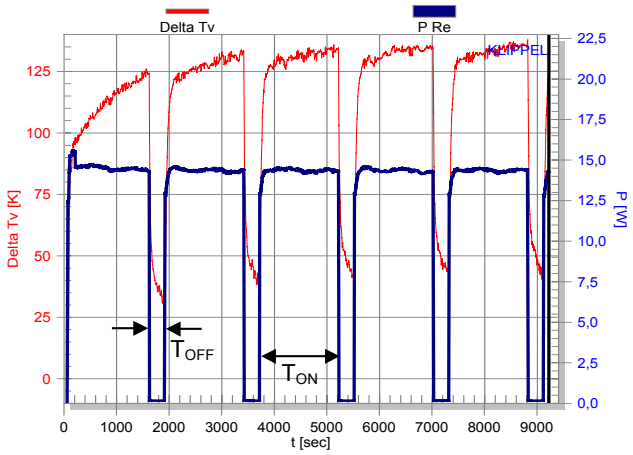

Fig. 26: Voice coil temperature ΔT_V (thin line) and Power P_{Re} (thick line) of a cycled f_1=1 kHz tone versus time.

In the last cycle of the test when the coil and magnet reached the thermal equilibrium we read the maximal voice coil temperature $\Delta T_{on}(f)$ at the beginning of the OFF-phase t_{s_off} for $f = f_1, f_2$ and f_3 as shown for the first measurement in Fig. 27. The short time constant of the voice coil τ_v causes the rapid decay at the beginning of the OFF-phase. The larger time constant τ_m of the magnet/frame structure causes an additional decay starting at later times. To separate both processes, the early decay is approximated by a straight line and the crossing point with the minimal temperature in the OFF-phase gives the slope time t_{slope}. At approximately 5 times of t_{slope} when the voice coil is in thermal equilibrium we read the temperature $\Delta T_{off}(f) = \Delta T_V(t_{s\_off} + 5t_{slope})$ for all three measurements.

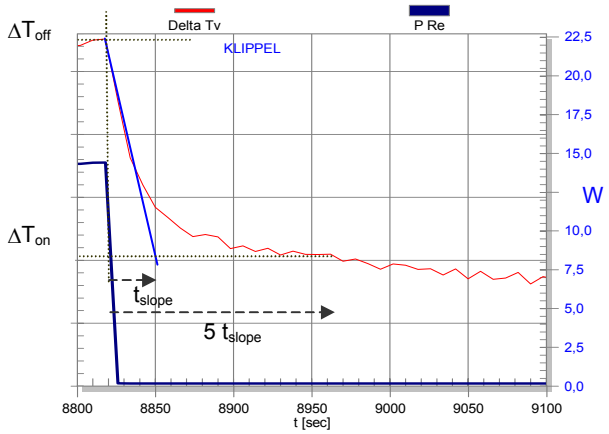

Fig. 27: Reading temperature T_{on} and T_{off} in the cooling phase of the last cycle.

6.3 Reading Time Constants

Using the result of the first power test the threshold temperature

$$\Delta T_{tau\_v}(t_{tau\_v}) = \Delta T_{TV}(t_{s\_off} + \tau_v) = 0.37\ \Delta T_{on}(f_1) + 0.63\ \Delta T_{off}(f_1) \quad (27)$$

is calculated where the time constant of the voice coil is elapsed.

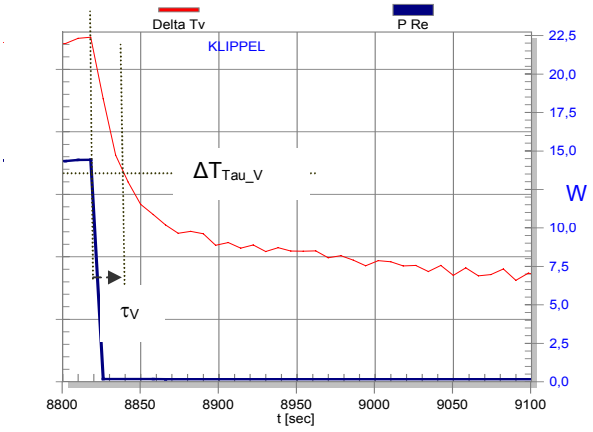

Fig. 28: Reading the time constant τ_v in the cooling phase

After reading the time t_{tau_v} in Fig. 28 when the temperature is decayed to ΔT_{tau_v} the time constant of the voice coil is calculated by

$$\tau_v = t_{tau\_v} - t_{s\_off} \quad (28)$$

Finally, the temperature threshold ΔT_{tau_m} is calculated where the time constant of the magnet is elapsed

$$\Delta T_{tau\_m} = \Delta T_V(t_{start} + \tau_m) = \Delta T_{on} - 0.37 * \Delta T_{off} \,. \tag{29}$$

After reading the starting time t_{start} and the time τ_{tau_m} when the voice coil temperature is equal to ΔT_{tau_m} the time constant

$$\tau_m = t_{tau\_m} - t_{start} \tag{30}$$

is calculated.

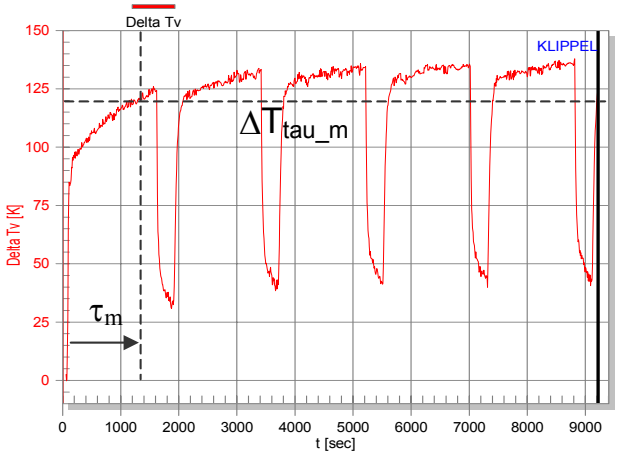

Fig. 29: Reading the time constant τ_m of the magnet.

6.4 Parameter Calculation

With the results of the previous measurements the thermal parameters can be calculated:

1. Power splitting coefficient

$$\alpha = -\frac{\varepsilon\, P_{\mathrm{Re}}(f_2) - P_{\mathrm{Re}}(f_1)}{\varepsilon\, P_{R2}(f_2) - P_{R2}(f_1)} \tag{31}$$

with the power dissipated in R_e and R_2 according Eqs. (17) and (19) and the ratio of the temperature variations

$$\varepsilon = \frac{\Delta T_{on}(f_1) - \Delta T_{off}(f_1)}{\Delta T_{on}(f_2) - \Delta T_{off}(f_2)} \tag{32}$$

measured at frequencies f_1 and f_2.

2. Thermal resistance of the magnet/frame structure

$$R_{tm} = \frac{\Delta T_{off}(f_1)}{P_{\mathrm{Re}}(f_1) + P_{R2}(f_1)} \frac{t_{on} + t_{off}}{t_{on}} \tag{33}$$

considering the long term mean power averaged over one cycle

3. Thermal resistance of the voice coil

$$R_{tv} = \frac{\Delta T_{on}(f_1) - \Delta T_{off}(f_1)}{P_{\mathrm{Re}}(f_1) + \alpha P_{R2}(f_1)} \tag{34}$$

considering both power sources

4. Thermal capacity of the voice coil

$$C_{TV} = \frac{\tau_{TV}}{R_{TV}} \tag{35}$$

5. Thermal capacity of the magnet structure

$$C_{TM} = \frac{\tau_M}{R_{TM}} \,. \tag{36}$$

6. Thermal resistance due to convection cooling

$$R_{tc} = \frac{1}{\dfrac{P_{\mathrm{Re}}(f_3)}{\Delta T_{on}(f_3)} - \dfrac{1}{R_{tv} + R_{tm}}} \tag{37}$$

7. Convection cooling parameter

$$r_c = \frac{1}{x_{rms}\, 2\pi f_3 R_{tc}} \tag{38}$$

6.5 Example

The measurement technique is applied to example driver A and the thermal parameters are listed in Table 2.

Parameter	*Value*	*Unit*
R_{tv}	5,9	K/W
C_{tv}	3,6	Ws/K
m_{copper}	9,7	g
R_{tm}	4,1	K/W
C_{tm}	272	Ws/K
m_{steel}	545	g
r_v	0,12	Ks^2/Wm^2
α	36	%
$R_e(T_a)$	1,88	Ω
R_2	7,97	Ω
L_2	0,23	mH
δ	0,00393	K^{-1}

Table 2: Thermal parameters of the driver A

Only a few parameters describe the thermal properties of the driver. Together with the nonlinear model we may predict the heat transfer and the resulting temperatures of the coil and magnet for any input signal having different spectral properties. This may be illustrated on the temperatures and powers during the three power tests as listed in Table 3. At 80 Hz the voice coil temperature ΔT_{on} is significantly lower than at 1kHz while almost the same input power P_{Re} is dissipated in R_e. The reason is that half of the power (γ=59 %) dissipated in R_e and R_2 flows directly into the convection cooling. Also at 16 kHz a significant part (γ=40 %) of the input power is directly transferred to the pole tips and does not contribute to the heating of the coil.

Measurement	**1st**	**2nd**	**3rd**	**Unit**
f	1000	16000	80	Hz
ΔT_{on}	138	130	52	K
ΔT_{off}	52	75	20	K
P_{Re}	14	4,8	13	W
P_{R2}	1,3	12,4	≈0	W
P_{coil}	14,6	9,3	5,2	W
P_{mag}	15,4	17,2	5,3	W
P_{con}	≈0	≈0	7,8	W
γ	5,3	46	60	%

Table 3: Voice coil temperatures and power splitting depending on the frequency of the test tone.

7 Optimal Thermal Design

Having a precise thermal model and a reliable measurement technique for the parameters we are able to assess design choices to improve the heat transfer and allow higher power handling. There are many ways in the literature such as using magneto fluid in the gap and providing special vents for ventilation in the pole plate. Here we discuss only the classical vent in the pole piece on the example driver B which is found on many drivers and illustrated in Fig. 30. The main purpose of this vent is to ventilate the space confined by dome, pole piece and voice coil former. This vent has an influence both on the electro-mechanical and on the thermal behavior of the driver.

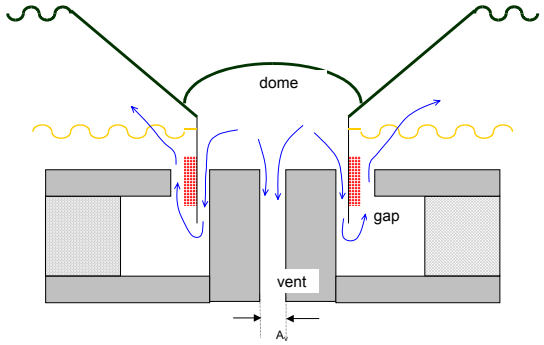

Fig. 30: Sectional View of a driver with vented back plate

Linear, nonlinear and thermal parameters have been measured of the original driver B with the open vent and on the modified driver with a completely sealed vent.

Fig. 31 shows the electrical impedances of the driver with open and sealed vent and Table 4 shows the variation of the linear parameters. Without any vent the enclosed air is pressed by the movement of the dome through the gap and the spider. The friction of the air flow in the gap increases the mechanical losses significantly. This reduces the electrical impedance at f_s and decreases the Q_{ms} from 8.5 down to 2.4. Since the electrical damping Q_{es}= 0.38 dominates the total loss factor Q_{ts}= 0.33, the overall performance of the driver is not changed significantly. This is also valid in the large signal domain where the $Q_{ts}(x)$ varies with voice coil displacement x due to the effect of the driver nonlinearites of Bl(x) and C_{ms}(x). Fig. 32 reveals that the $Q_{ts}(x)$ doubles for a moderate displacement x_{peak}= 4 mm whereas the difference caused by the driver modification is much smaller. Sealing the vent neither produced audible noise due to turbulences in the gap nor increased the nonlinearities of the compliance.

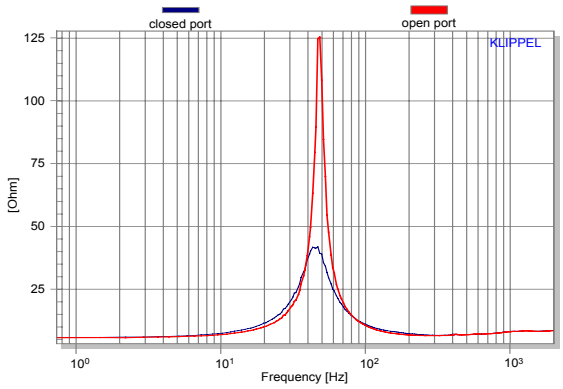

Fig. 31: Electrical input impedance of the original driver with open vent (thick line) and of the modified driver with sealed vent (thin line).

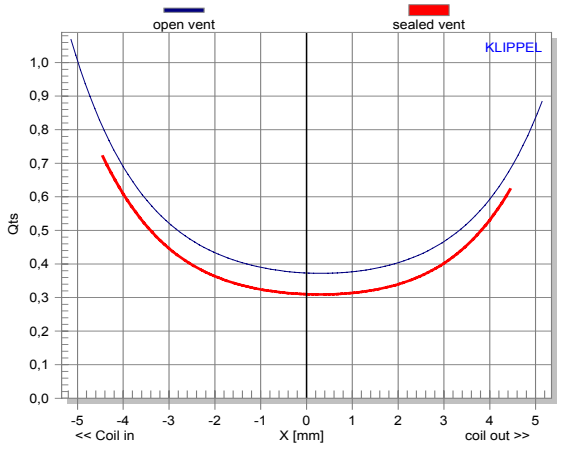

Fig. 32: Total loss factor $Q_{ts}(x)$ versus displacement x considering nonlinearities of driver B with open or sealed vent.

Parameters	*Vent open*	*Vent sealed*	*unit*
Re	5.72	5.78	Ohm
Le	0.089	0.092	mH
L2	0.773	0.730	mH
R2	2.84	2.81	Ohm
fs	48.0	45.0	Hz
Mms	14.744	14.843	g
Rms	0.523	1.756	kg/s
Cms	0.75	0.84	mm/N
Kms	1.34	1.19	N/mm
Bl	8.00	7.99	N/A
Qms	8.51	2.39	
Qes	0.40	0.38	
Qts	0.38	0.33	

Table 4: Linear parameters of the driver B with open and sealed vent and the rear pole plate.

After measuring the linear and nonlinear parameters the effect on the thermal parameters is investigated. Using the two-tone technique described above the parameters $R_{tc}(v)$ and $R_{ta}(x)$ are measured on driver B with and without port sealing by having compariable amplitudes of the voice coil displacement. One tone at 2 kHz was used for heating while the second tone was varied between 5 Hz and 200 Hz to investigate the influence of the voice coil displacement. For the vented and sealed case the predicted curves in Fig. 33 and Fig. 34, respectively, agree very well with the measured curves. However, the driver with the sealed vent has a significantly lower total resistance $R_{tc}(v) + R_{ta}(x)$.

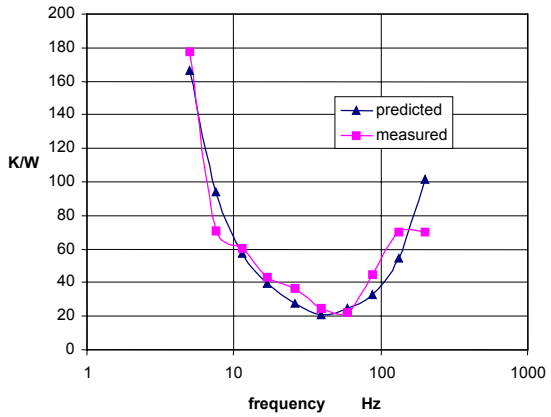

Fig. 33: Measured and predicted total resistance $R_{tc}+R_{ta}$ of the original driver B with open vent

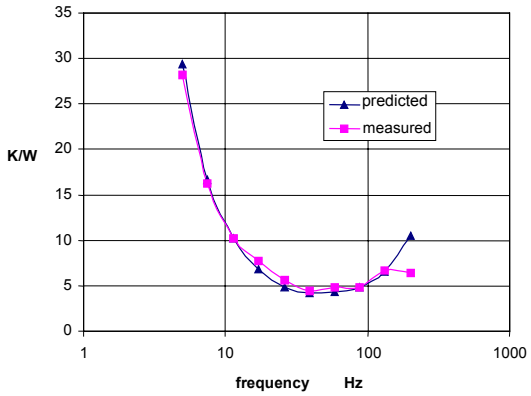

Fig. 34: Measured and predicted total resistance $R_{tc}+R_{ta}$ of the modified driver B with sealed vent

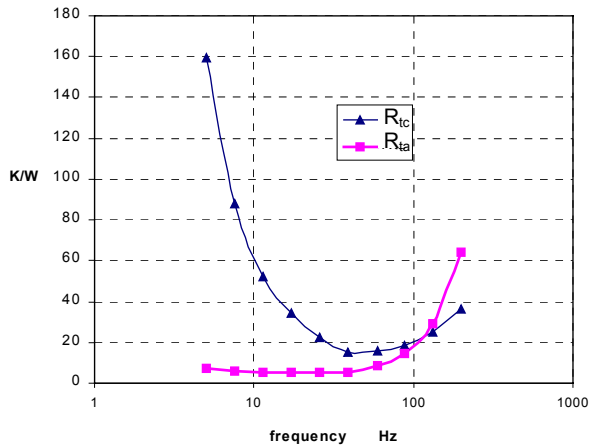

Fig. 35: Thermal resistances $R_{tc}(v)$ and $R_{ta}(x)$ versus frequency f_1 of the original driver B with open vent

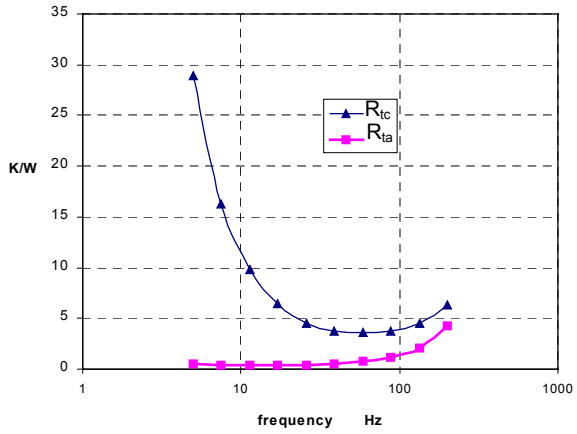

Fig. 36: Thermal resistances $R_{tc}(v)$ and $R_{ta}(x)$ versus frequency f_1 of the modified driver B with sealed vent

The differences in the convection cooling become more obvious in Fig. 35 and Fig. 36 showing the thermal resistance $R_{tc}(v)$ and $R_{ta}(x)$, separately. The thermal resistance $R_{tv}(v)$ has a minimum at the resonance frequency f_s where the cone velocity v is maximal. However, the minimal R_{tv} of the driver with the closed vent in Fig. 36 is only a quarter of the value measured with the open vent. Obviously, sealing of the vent removes the bypass of the air flow and forces all the air through the gap and increases the volume velocity at the coil's surface.

The resistance $R_{ta}(x)$ is also significantly higher in the original driver with the unsealed vent. Thus the exchange of air in the gap is quite poor while the driver with sealing also provides an efficient pumping mechanism.

The lower the resistances $R_{tc}(v)$ and $R_{ta}(x)$ the more power will bypass the voice coil. The power bypass factor γ in Fig. 37 reveals that up to 50 % of the input power will not contribute to the heating of the coil in the modified driver with the sealed vent. The convection cooling in the original driver can transfer 17 % directly to the ambience.

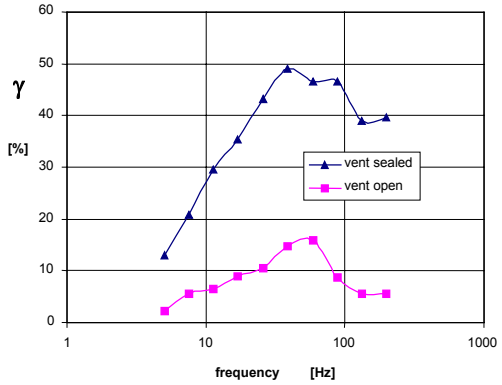

Fig. 37: Bypass power factor γ versus frequency of the excitation tone for the driver with and without vent

Since the influence of the vent on the mechanical and acoustical system is relatively small and causes no unpleasant effects, sealing the vent would bring a significant benefit in power handling for the particular example. However, this can not be generalized for all drivers. If the diameter of the coil is large and the relative variation of the volume below the dust cap becomes high, the nonlinear compliance of the enclosed air may increase harmonic distortion The asymmetrical characteristic may also generate a DC-component in the voice coil displacement, shifting the coil in a positive direction to the compliance maximum (away from the back-plate). A high velocity in the gap may also generate additional noise due to turbulences. Thus we have to make the vent's area A_v as small as possible to exploit the convection cooling and as large as necessary to avoid the nonlinear effects. In this trade-off the dependence of the convection parameter on the sectional area A_v of the vent

$$r_v(A_v) = \frac{r_{vs}}{\left(\frac{r_{vs}}{r_{vo}} - 1\right)\frac{A_v}{A_{vo}} + 1} \tag{39}$$

can be calculated by using the parameters r_{vo} and r_{vs} measured at a driver with open vent area A_{vo} and the same driver with a sealed vent, respectively.

For our example driver B Fig. 38 shows the dependency of the convection parameter r_v versus surface area A of the vent. At small areas most of the air will be pumped through the gap and the convection parameters becomes maximal and at large areas the bypass through the vent is dominant and convection cooling is negligible. Choosing an area just before the decay of r_v at about 5 – 10 mm^2 will preserve high convection cooling but will avoid a nonlinear compression of the air. Noise due to turbulences should be avoided by using multiple vents (probably made in the pole plate) with rounded edges at the mouth.

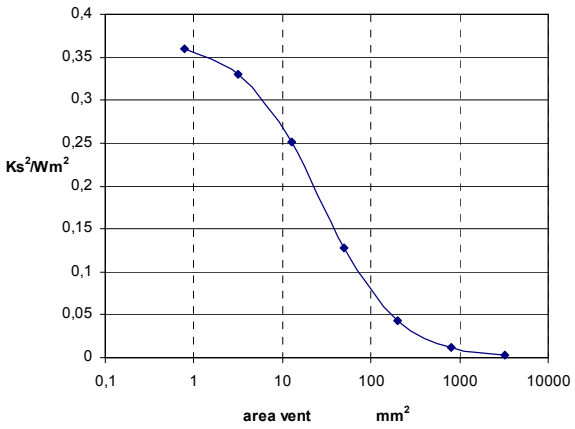

Fig. 38: Dependency of the convection parameter $r_v(A_v)$ versus sectional area A_v of the vent for example driver B.

8 Conclusion

In the large signal domain where the heating of the coil is a relevant issue, the driver nonlinearities $Bl(x)$, $C_{ms}(x)$ and $L_e(x)$ and the convection have a dramatic influence on the voice coil temperature T_v. Thus we need a nonlinear model for both the electrical-mechanical and thermal mechanisms and have to consider the complicated interactions. An equivalent circuit with lumped elements having nonlinear parameters is introduced which is a natural extension of the traditional modeling. This model has been verified on a couple of loudspeakers. The free parameters of the model can be identified for a particular driver by a simple technique also suggested in this paper.

The model with identified parameters allows a better prediction of the voice coil temperature and other state variables of the loudspeaker for any audio input. It can be easily implemented in a numerical simulation tool for loudspeaker design or in digital controllers.

The modeling, prediction and measurement gave a valuable insight in the heat transfer in loudspeakers:

The convection cooling and the direct heat transfer to the magnet/pole tips due to eddy currents are important bypasses reducing the heating of the coil. The fraction of power which is not seen by the coil can be expressed by a convenient bypass factor γ which should be optimized in practical design.

The nonlinear parameters $Bl(x)$ and $C_{ms}(x)$ decrease the electrical input impedance and increase the input power of the speaker. The nonlinearities also cause a compression of the displacement amplitude which impairs the natural convection cooling. Both effects contribute to the heating of the coil significantly.

Air convection cooling is a very complex process. The most dominant mechanism is the heat transfer between coil surface and air layer surrounding the coil. The resistance of this path depends on the velocity. Since the thermal capacity of the air layer is negligible we need some air exchange. Fortunately, high voice coil velocity producing some voice coil displacement pumping enough air to the ambience.

A simple form of forced convection cooling can be realized by pumping the air below the dust cap through the gap. Large coil diameter and small clearance of the coil in the gap will increase the air velocity. Unfortunately a trade-off with the linear and nonlinear performance of the mechanical system is required.

9 References

[1] G. Behler, A. Bernhard, "Measuring Method to derive the Lumped Elements of the Loudspeaker Thermal Equivalent Circuit," presented at the 104th Convention 1998 May 16-19, Amsterdam, preprint #4744.

[2] G. Behler, "Measuring the Loudspeaker's Impedance During Operation for the Derivation of the Voice Coil Termperature," presented at the 98th Convention 1995 February 25-28, Paris, preprint #4001.

[3] Henricksen, "Heat Transfer Mechanisms in Loudspeakers: Analysis, Measurement and Design, " J. Audio Eng. Soc. Vol 35. No. 10 , 1987 October.

[4] D. Button, Heat Dissipation and Power Compression in Loudspeakers, J. Audio Eng. Soc., Vol. 40, No1/2 1992 January/February.

[5] C. Zuccatti, Thermal Parameters and Power Ratings of Loudspeakers, J. Audio Eng. Soc., Vol. 38, No. 1,2, 1990 January/February.

[6] "Measurement of Nonlinear Thermal Loudspeaker Parameters, " Application note AN19, KLIPPEL GmbH, www.klippel.de.